Freescale Semiconductor
Application Note

56F80x Resolver Driver and Hardware Interface

Describes the 56F80x Resolver Driver and
Hardware Interface and Shows an Example of
Driver Use

Martin Mienkina, Pavel Pekarek, Frantisek Dobes

1. Introduction

Resolver position sensors resemble small motors and are essentially rotary transformers so the coefficient of coupling between rotor and stator varies with shaft angle. A resolver is based on the concept of encoding the shaft angle into sine and co-sine signals.

This Application Note describes a solution for obtaining the estimations of actual angle and speed of the resolver. A theoretical analysis, proposal of the Resolver-to-Digital (R/D) hardware interface and a design of the device software driver are mentioned here. The software driver is written in C language using powerful intrinsic functions. It provides estimations of rotor angle and speed to be achieved to 10-bit accuracy at a CPU load of 7.5% (8KHz update rate). Finally, a brief description is given for both an example of driver use and some experimental results. It is demonstrated that the 56F80x is suitable for high-end vector control applications utilizing the resolver position sensor.

2. Features of Freescale's Digital Signal Controllers (DSCs)

The Freescale 56F80x family is well suited for digital motor control and data processing, combining the DSP's calculation capability with MCU's controller features on a single chip. This arises from the high-speed cores of the devices and a number of architectural features. Typically, Freescale's DSCs offer many dedicated peripherals, such as Pulse Width Modulation (PWM) units, Analog-to-Digital Converters (ADC), Timers, communication peripherals (SCI, SPI, CAN), on-board Flash and RAM.

Contents

Several members of the family are available, including the 56F801, 56F803, 56F805 and 56F807, each with various peripheral sets and on-board memory configurations.

A typical member of the family, the 56F805, provides the following peripheral blocks:

- 12-bit Analog to Digital Converters (ADCs), supporting two simultaneous conversions with dual 4-pin multiplexed inputs, ADCs can be synchronized by the PWM modules
- Two Pulse Width Modulator modules (PWMA & PWMB), each with six PWM outputs, three Current Sense inputs, and four Fault inputs, fault tolerant design with deadtime insertion, supporting both Center- and Edge- aligned modes
- Two Quadrature Decoders (Quad Dec0 & Quad Dec1), each with four inputs, or two additional Quad Timers A & B
- Two dedicated General Purpose Quad Timers totalling 6 pins: Timer C with 2 pins and Timer D with 4 pins
- A CAN 2.0 A/B Module with 2-pin ports used to transmit and receive
- Two Serial Communication Interfaces (SCI0 & SCI1), each with two pins, or four additional GPIO lines
- A Serial Peripheral Interface (SPI), with configurable 4-pin port, or four additional GPIO lines
- A Computer Operating Properly (COP) Watchdog timer
- Two dedicated external interrupt pins
- 14 dedicated General Purpose I/O (GPIO) pins, 18 multiplexed GPIO pins
- An external reset pin for hardware reset
- A JTAG/On-Chip Emulation (OnCE)
- A software-programmable, Phase Lock Loop-based frequency synthesizer for the core

Table 2-1.   Memory Configuration

	56F801	56F803	56F805	56F807
Program Flash	8188 x 16-bit	32252 x 16-bit	32252 x 16-bit	61436 x 16-bit
Data Flash	2K x 16-bit	4K x 16-bit	4K x 16-bit	8K x 16-bit
Program RAM	1K x 16-bit	512 x 16-bit	512 x 16-bit	2K x 16-bit
Data RAM	1K x 16-bit	2K x 16-bit	2K x 16-bit	4K x 16-bit
Boot Flash	2K x 16-bit	2K x 16-bit	2K x 16-bit	2K x 16-bit

The resolver driver utilizes two ADC channels and one timer of the 56F80x. In this particular application, the ADC channels must be configured to sample both sine and co-sine signals simultaneously. The timer provides the generation of the square wave signal. This signal is further conditioned by external hardware to the form, which is convenient for excitation of the resolver. The controller estimates the actual angle of the rotor shaft on the basis of the measured sine and co-sine signals of the resolver. However, the controller is not only dedicated to realization of the R/D conversion, hence the software driver of the resolver has to be designed in a way to be able to link and operate within an existing application (e.g., a PMSM vector control application).

The accuracy of the rotor angle and speed estimations greatly depends on features of the ADC. Particularly, ADC accuracy, resolution and set of possible operation modes are crucial for achieving the higher accuracy estimations. To provide a comprehensive description of the R/D conversion and show its real implementation, a brief survey of features of the appropriate ADC is given here.

- 12-bit resolution with a sampling rate up to 1.66 million samples per second
- Maximum ADC Clock frequency of 5MHz with a 200ns period
- Single conversion time of 8.5 ADC Clock cycles (8.5 x 200ns = 1.7us)
- Additional conversion time of 6 ADC clock cycles (6 x 200ns = 1.2us)
- Eight conversions in 26.5 ADC Clock cycles (26.5 x 200ns = 5.3us) using Simultaneous mode
- ADC can be synchronized to the PWM or via the SYNC signal
- Simultaneous or Sequential sampling
- Internal multiplexer to select two of eight inputs
- Ability to sequentially scan and store up to eight measurements and simultaneously sample and hold two inputs
- Optional interrupts at end of scan, if an out-of-range limit is exceeded, or at zero crossing
- Optional sample correction by subtracting a pre-programmed offset value
- Signed or unsigned result
- Single ended or differential inputs

There are two separate converters available on 56F801, 56F803 and 56F805, each associated with four analog inputs and providing two channels to be sampled simultaneously. The 56F807 has four separate converters, each having four inputs and therefore achieving four channels to be sampled simultaneously. The results of conversions are stored for further post-processing in readily accessible registers. The conversion process may be either initiated by the SYNC signal or by setting the START bit of the ADC Control Register (ADCR).

3. Resolvers

Resolvers may be considered as inductive position sensors which have their own rotor and stator windings shifted by 90°.
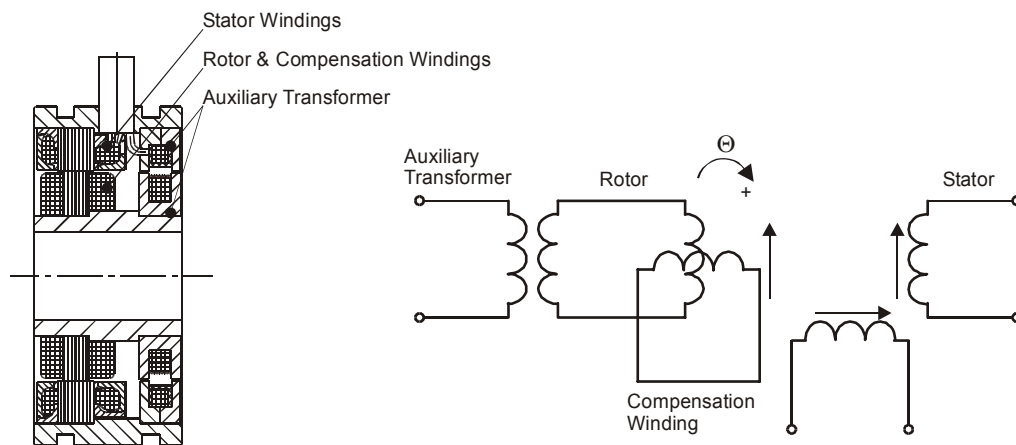
Figure 3-1.   Block Scheme of the Hollow Shaft Resolver

The majority of resolvers used nowadays are referred to as *Hollow Shaft Resolvers*. They transfer energy from stator to rotor by means of an auxiliary rotary transformer (see **Figure 3-1**). The resolver rotor is directly mounted on the motor shaft and the resolver stator is fixed to the motor shield. Note that these resolver parts have to be concentrically fastened with the longitudinal axis of the motor shaft. Ordinarily, a concentricity of resolver rotor against stator up to 0.05 mm is needed, otherwise resolver parameters might deteriorate. Thanks to the absence of bearings and brushes the life-cycle of *Hollow Shaft Resolvers* is practically unlimited.

3.1 Resolver Parameters

This section lists the principal resolver parameters, which should be considered seriously during the development stage of the software driver and hardware interface. These parameters are the following:

1. **Electrical Error** - determines the accuracy of the measurement of rotor angle and frequently varies from $\pm 3'$ to $\pm 15'$. Standard *Hollow Shaft Resolvers* have an electrical error of up to $\pm 10'$.

2. **Transformation Ratio** - defines ratio between output and input voltage. This ratio is practically maintained in a range of 0.5 $\pm 5\%$; however, it may be set at a wide range, e.g., 0.25-1.0.

3. **Input Voltage, Current and Frequency** - usually from 4 to 30 V_{rms}, from 20 to 100mA and from 400Hz up to 10kHz. It should be noted that *Electrical Error* and *Transformation Ratio* are independent parameters of the *Input Voltage* and *Current and Frequency*, at a wide range.

4. **Null Voltage** - denotes the content of disturbance and orthogonal voltage components of the resolver (commonly lower than 20mV) at zero output voltage.

5. **Phase Shift** - refers to a phase shift between excitation of the resolver and its output signals. Regarding 2-Phase resolvers, it frequently varies within $\pm 10°$. Note that this parameter should be taken into account seriously during hardware and software implementation of the R/D conversion, as will be discussed in **Section 4.**

6. **Stator and Rotor Resistance** - R_S, R_R

7. **Short-Circuit and No-Load Stator and Rotor Impedances** - Z_{SS}, Z_{SO}, Z_{RS}, Z_{RO}

The resolver output voltage amplitudes correspond to sine and co-sine of the rotor angle Θ, as shown in **Figure 3-2**. Note that these voltages can be expressed in terms of the actual rotor angle Θ:

$$U_{S1S3} = K\ U_{R2R4}\ \sin\Theta \qquad\qquad (EQ\ 3\text{-}1)$$

$$U_{S2S4} = K\ U_{R2R4}\ \cos\Theta \qquad\qquad (EQ\ 3\text{-}2)$$

where K is the *Transformation Ratio*, and $U_{R2R4} = U_{MAX}\sin(\omega t)$ is an instantaneous excitation voltage applied on the auxiliary transformer winding. Note that the instantaneous excitation voltage U_{R2R4} has an amplitude U_{MAX} and operates at angular frequency $\omega = 2\pi f$. The instantaneous excitation voltage U_{R2R4} will be further referred to as a reference voltage U_{ref}. The output resolver voltages U_{S1S3}, U_{S2S4} will be further referred to as U_{sin}, U_{cos}, respectively.
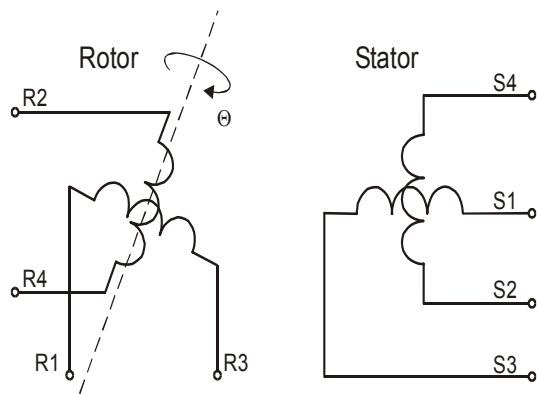
Figure 3-2.   Block Scheme of the Resolver

3.2 Theory of Resolver Operation

The resolver is basically a rotary transformer with one rotating reference winding (supplied by U_{ref}) and two stator windings. The reference winding is fixed on the rotor, and therefore, it rotates jointly with the shaft passing the output windings, as is depicted in **Figure 3-3**. Two stator windings are placed in quadrature of one another and generate the sine and co-sine voltages U_{sin}, U_{cos}, respectively. Note that the sine winding is phase advanced by 90° with respect to co-sine winding. Both windings will be further referred to as output windings.
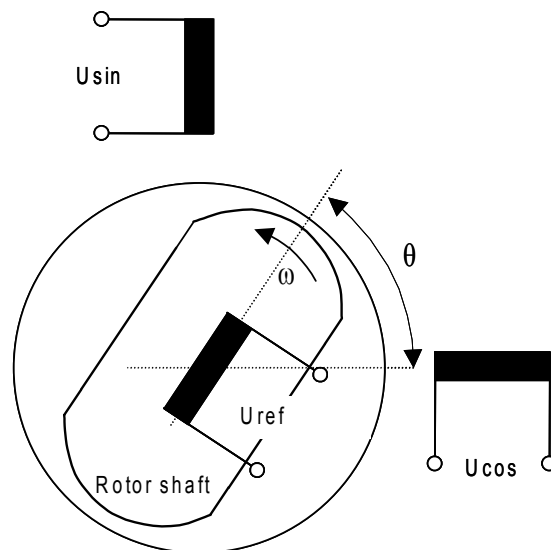
Figure 3-3.   Resolver Basics

In consequence of the excitement applied on the reference winding U_{ref} and along with the angular movement of the motor shaft Θ, the respective voltages are generated by resolver output windings U_{sin}, U_{cos} (see **Figure 3-4**).

56F80x Resolver Driver and Hardware Interface, Rev. 1
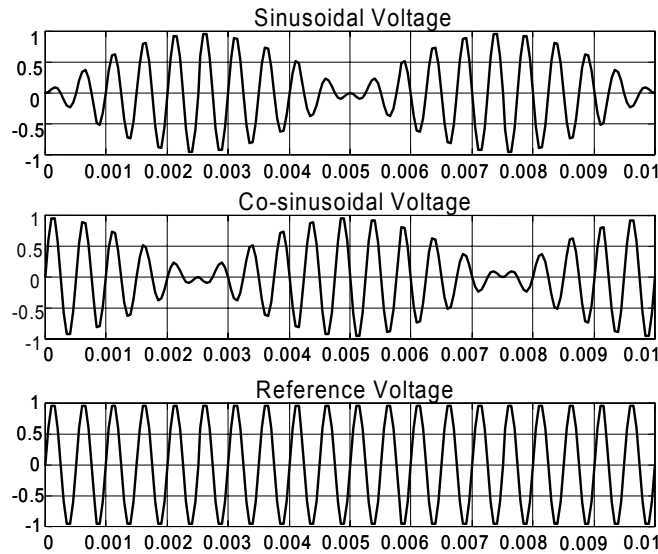
Figure 3-4.   Excitation and Output Signal of the Resolver

The frequency of the generated voltages is identical to the reference voltage and their amplitudes vary according to the sine and co-sine of the shaft angle Θ. Considering that one of the output windings is aligned with the reference winding, then it is generated full voltage on that output winding and zero voltage on the other output winding and vice versa. The rotor angle Θ can be extracted from these voltages using a digital approach as will be discussed in the next section.

3.3   Basics of Angle Extraction

Formerly resolvers were used primarily in analog design in conjunction with a *Resolver Transmitter - Resolver Control Transformer* [1]. These systems were frequently employed in servomechanisms, e.g. in aircraft on board instrument systems. Modern systems, however, use the digital approach to extract rotor angle and speed from the resolver output signals. The most common solution is either a *Trigonometric* or *Angle Tracking Observer* method. It should be noted that both methods require fast and high accuracy measurement of the resolver output signals to be carried out.

3.3.1   Trigonometric

The shaft angle can be determined by an *Inverse Tangent* function of the quotient of the sampled resolver output voltages U_{sin}, U_{cos}. This determination can be expressed, in terms of resolver output voltages, as follows:

$$\Theta = atan\left(\frac{U_{sin}}{U_{cos}}\right)$$

(EQ 3-3)

An indispensable precondition of the accurate rotor angle estimation is to sample the resolver output signals simultaneously and close to their period peaks (see **Figure 3-5**).

$$\text{atan}\left(\frac{U_{sin}}{U_{cos}}\right) \quad \Theta$$
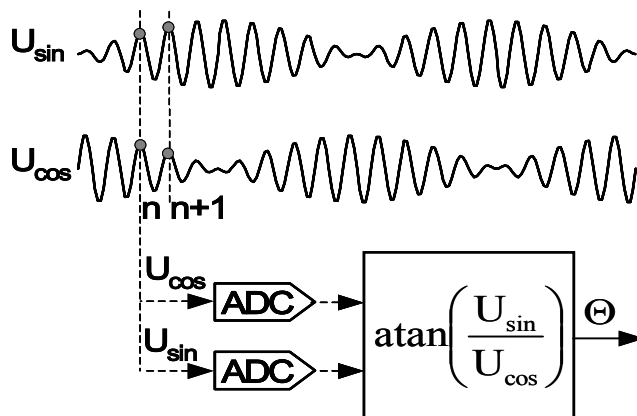
Figure 3-5.   Angle Extraction Using the Inverse Tangent Method

Note that modern control algorithms for electric drives require knowledge of the rotor angle and the rotor speed. The *Trigonometric* method, however, only yields values of the unfiltered rotor angle without any speed information. Therefore, for a final application, it is often required that a speed calculation with smoothing capability be added. This drawback might readily be eliminated if a special *Angle Tracking Observer* is utilized. This method is discussed in the next section.
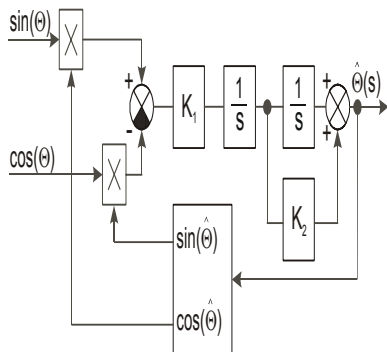
3.3.2 Angle Tracking Observer

The second method (algorithm), widely used for estimation of the rotor angle and speed, is generally known as an *Angle Tracking Observer* (see **Figure 3-6**).
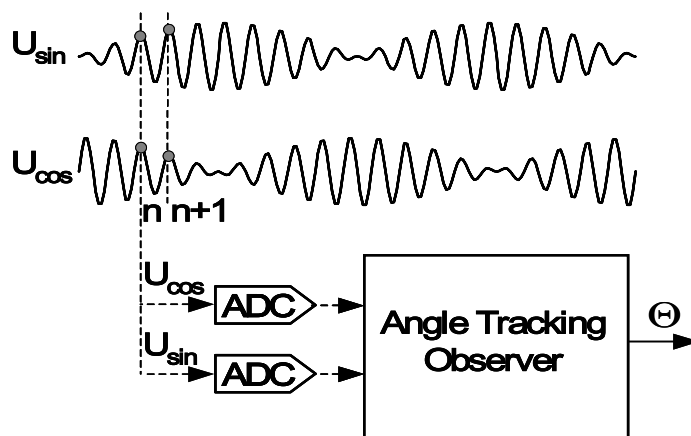
Figure 3-6.   Angle Extraction Using the Angle Tracking Observer

A great advantage of the *Angle Tracking Observer* method, compared to the *Trigonometric* method, is that it yields smooth and accurate estimations of both the rotor angle and rotor speed [2].

The *Angle Tracking Observer* compares values of the resolver output signals U_{sin}, U_{cos} with their corresponding estimations $\hat{U}_{sin}$, $\hat{U}_{cos}$. As in any common closed-loop systems, the intent is to minimize observer error. The observer error is given here by subtraction of the estimated resolver rotor angle $\hat{\Theta}$ from the actual rotor angle Θ (see **Figure 3-7**).
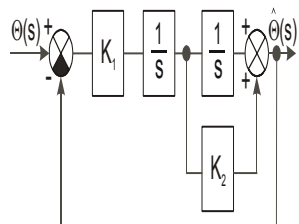

Figure 3-7.   Block Scheme of the Angle Tracking Observer

Note that mathematical expression of observer error is known as the formula of the difference of two angles:

$$\sin(\Theta - \hat{\Theta}) = \sin(\Theta)\cos(\hat{\Theta}) - \cos(\Theta)\sin(\hat{\Theta}) \tag{EQ 3-4}$$

where $\sin(\Theta - \hat{\Theta})$ denotes observer error, Θ is the actual rotor angle and $\hat{\Theta}$ is its corresponding estimation.

In case of small deviations of the estimated rotor angle compared to the actual rotor angle, the observer error may be considered in the form $\Theta - \hat{\Theta}$.

Figure 3-8.   Simplified Block Scheme of the Angle Tracking Observer

The main benefit of the *Angle Tracking Observer* utilization, in comparison with the *Trigonometric* method, is its smoothing capability. Smoothing is achieved by the integrator and PI controller, which are connected in series and closed by a unit feedback loop, see the block diagram in **Figure 3-8**. This block diagram nicely tracks actual rotor angle and speed and continuously updates their estimations.

The *Angle Tracking Observer* transfer function is expressed, with the help of its simplified block scheme in **Figure 3-8**, as follows:

$$F(s) = \frac{\hat{\Theta}(s)}{\Theta(s)} = \frac{K_1(1 + K_2 s)}{s^2 + K_1 K_2 s + K_1} \tag{EQ 3-5}$$

The characteristic polynomial of the *Angle Tracking Observer* corresponds to the denominator of transfer function **EQ 3-5**:

$$s^2 + K_1 K_2 s + K_1 \qquad \text{(EQ 3-6)}$$

Appropriate dynamic behavior of the *Angle Tracking Observer* may be achieved by placement of the poles of the characteristic polynomial. This general method is based on matching the coefficients of the characteristic polynomial with the coefficients of the general second-order system $G(s)$:

$$G(s) = \frac{\omega_n^2}{s^2 + 2\zeta\omega_n s + \omega_n^2} \qquad \text{(EQ 3-7)}$$

where ω_n is the *Natural Frequency* $[\text{rad s}^{-1}]$ and ζ is the *Damping Factor* $[-]$. Once the desired response of the general second-order system $G(s)$ is found, the *Angle Tracking Observer* coefficients K_1, K_2 can be calculated using these expressions:

$$K_1 = \omega_n^2 \qquad \text{(EQ 3-8)}$$

$$K_2 = \frac{2\zeta}{\omega_n} \qquad \text{(EQ 3-9)}$$

The *Angle Tracking Observer* transfer function is a second order and has one zero. This real-axis zero affects the residue, or amplitude, of a response component but does not affect the nature of the response - exponential damped sine. It can be proven that the closer the zero is to the dominant poles, the greater its effect is on the transient response. As the zero moves away from the dominant poles the transient response approaches that of the two-pole system [3], [4].

The transient responses of the *Angle Tracking Observer* to a 180° step change of the actual rotor angle, given by simulation of the transfer function **EQ 3-5**, are discussed thereinafter. These simulations have been carried out for two sets of *Angle Tracking Observer* coefficients. It is shown that both coefficient sets have enabled the *Angle Tracking Observer* to reach a steady state value within a *Settling Time*[1] < 15 ms and with a *Peak Overshoot*[2] < 17 %. It should be noted that such large step changes could never happen in a real application due to the continuous minimization of observer error. In reality, possible step changes are much smaller (compared to 180°) so a steady state is reached much faster.

3.3.3 Selecting Optimal Observer Coefficients

This application note discusses two coefficient sets. The first set of coefficients was chosen to perform optimal smoothing of the rotor angle and speed estimations. On the contrary, the second set of coefficients was selected to minimize the *Settling Time*. The next paragraph gives an overview of the utilized observer parameters and shows some results of the *Angle Tracking Observer* simulations - all simulations were pursued using Matlab software. The simulation models were solved using "Euler-Forward Integration" with an integration step $62.5\,\mu s$.

---

1. The time taken for the response to reach and remain within a specified range of its final value. An allowable tolerance of $\pm 20'$ (electrical) has been considered. This tolerance roughly matches an estimation error of ± 1 LSB when a 10-bit resolution is used for angle measurement.
2. The amplitude of the first peak normally expressed as a percentage of the final (steady-state) value.

In the first case, the coefficients of the *Angle Tracking Observer* have been originated on the parameters of the general second-order system $\omega_n = 500\,\text{rad s}^{-1}$, $\zeta = 0.4, 0.84, 1.2 \text{ and } 1.6$. On the basis of these parameters, the coefficients of the *Angle Tracking Observer* $K_1 = 250000$, $K_2 = 0.0016, 0.00336, 0.0048 \text{ and } 0.0064$ were calculated using **EQ 3-8** and **EQ 3-9**. The corresponding simulation results are shown in **Figure 3-9**.
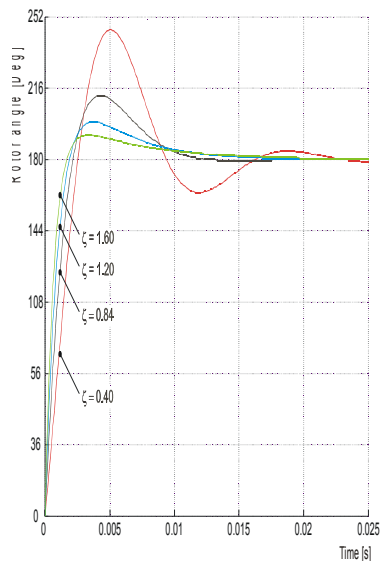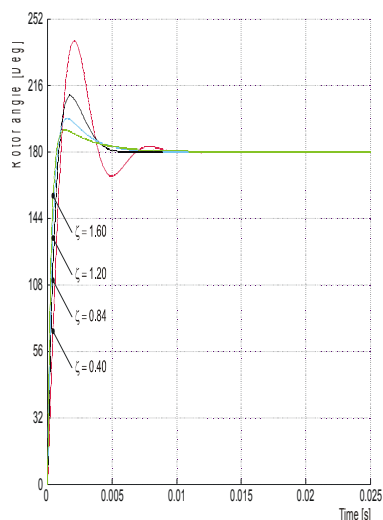

Figure 3-9. Dynamic Responses of the Rotor Angle Estimations -
$\omega_n = 500\,\text{rad s}^{-1}$, $\zeta = 0.4, 0.84, 1.2 \text{ and } 1.6$

This figure clearly illustrates that the minimal possible *Settling Time,* $t_S = 0.013\text{s}$, is achieved with the *Natural Frequency* $\omega_n = 500\,\text{rad s}^{-1}$ and the *Damping Factor* $\zeta = 0.84$. Note that for this setting the *Angle Tracking Observer* generates the *Peak Overshoot* $OV = 17\,\%$ in the transient response of the estimated rotor angle. This selection of the *Natural Frequency* and the *Damping Factor* yields a good smoothing capability of the *Angle Tracking Observer*, see **Section 5.3** for more details.

In the second case, the coefficients of the *Angle Tracking Observer* were based on the parameters of the general second-order system $\omega_n = 1200\,\text{rad s}^{-1}$, $\zeta = 0.4, 0.84, 1.2 \text{ and } 1.6$. The resulting coefficients of the *Angle Tracking Observer* $K_1 = 1440000$ and $K_2 = 0.0006, 0.0014, 0.002 \text{ and } 0.0026$ were found with the help of equation **EQ 3-8** and **EQ 3-9**, respectively. The simulation results that correspond to this particular setting of the *Angle Tracking Observer* are shown in **Figure 3-10**.

Figure 3-10.   Dynamic Responses of the Rotor Angle Estimations -

$\omega_n = 1200\,\text{rad s}^{-1}$, $\zeta = 0.4, 0.84, 1.2 \text{ and } 1.6$

Note that the minimal *Settling Time*, $t_S = 0.0053s$, is achieved with the *Natural Frequency* $\omega_n = 1200 \text{ rad s}^{-1}$ and the *Damping Factor* $\zeta = 0.84$. The *Angle Tracking Observer*, having been based on the dynamic parameters of the general second-order system, generates the *Peak Overshoot* $OV = 17\%$. This selection of the *Natural Frequency* reasonably shortens the *Settling Time*, however it also decreases the smoothing capability of the *Angle Tracking Observer*.

By considering **Figure 3-9** and **Figure 3-10**, the following conclusions may be reached relating to the selection of the coefficients of the *Angle Tracking Observer*:

- The *Settling Time* of the transient response greatly depends on the *Natural Frequency*; i.e., any higher values of the *Natural Frequency* shorten the *Settling Time* and vice versa. Note that the *Peak Overshoot* does not depend on the *Natural Frequency*.

- The *Peak Overshoot* only depends on the *Damping Factor*; i.e., any lower values of the *Damping Factor* increase the *Peak Overshoots*. Note that considerable changes in the *Damping Factor* only slightly influence the *Settling Time*.
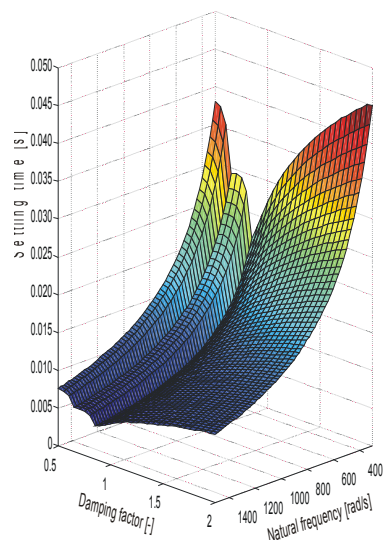
The impact of the *Natural Frequency* and *Damping Factor* on the dynamic behavior of the *Angle Tracking Observer* is clearly summarized in **Figure 3-11**, **Figure 3-12**.

Figure 3-11 graphically illustrates variations in the *Peak Overshoot* (z-axis) in terms of changes made to the *Natural Frequency* and the *Damping Factor*. In this figure, the x-axis represents the *Natural Frequency*, expressed in rad s^{-1}, and the y-axis the dimensionless *Damping Factor*. The *Natural Frequency* and *Damping Factor* vary in the ranges $300 \text{ rad s}^{-1} \le \omega_n \le 1500 \text{ rad s}^{-1}$ and $0.5 \le \zeta \le 2.5$, respectively.
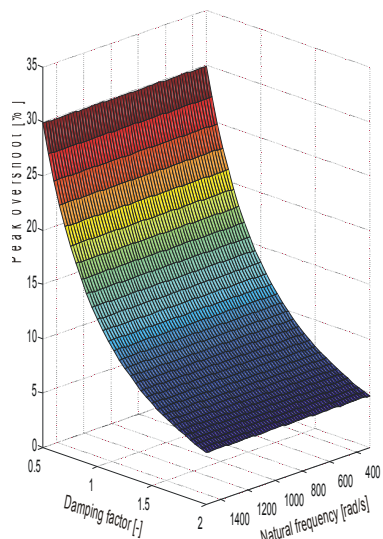
Figure 3-11.   Peak Overshoot as a Function of Natural Frequency and Damping Factor

Figure 3-12 graphically illustrates variations in the *Settling Time* (z-axis) in terms of changes of the *Natural Frequency* and the *Damping Factor*. The x and y-axes represent the variations of the *Natural Frequency* and *Damping Factor*, respectively.

Figure 3-12.   Settling Time as a Function of Natural Frequency and Damping Factor

This figure clearly shows the *Damping Factor* $\varsigma = 0.84$, at which the *Settling Time* of the *Angle Tracking Observer* is minimized.

This section has given a detailed description of the methods of angle extraction. Two methods, *Trigonometric* and *Angle Tracking Observer*, have been addressed and theoretically analyzed. Theoretical analysis shows that the *Angle Tracking Observer* algorithm performs a better estimation of the rotor angle and speed than the *Trigonometric* method. Because of this fact, the final resolver software driver exploits the *Angle Tracking Observer* algorithm.

4. Hardware Interface

An interface for direct connection of the resolver position sensor with the 56F805EVM is discussed here. This interface circuit generates/shapes the signal for the resolver reference winding and conditions signals from sin/cos windings for measurement by the on chip ADC module.

The interface circuit in **Figure 4-1** consists of two main parts:

- • Resolver driving circuitry
- • Resolver sin/cos signals conditioning circuitry

The resolver driving circuitry shapes a rectangular reference signal from the controller Quad Timer (channel TD1) output to a sinusoidal waveform. U1A creates an integrator which transforms the rectangular signal into a triangle. The remaining higher harmonic component is filtered out by the following stage U1B that drives the resolver reference winding. The U1B stage is, in fact, an integrator too. The ratios of R1/R3 and R2/R4 resistors control the integrator's linearity; the higher the ratio the better the sine curve generated at the output. However, if the ratio is too high the circuitry is sensitive to noise pickups from the power stages and also to changes in the reference signal duty cycle. Therefore, the reference signal is automatically generated by the Quad Timer module (channel TD1) to achieve a precise 50% duty cycle for a quality reference signal.

The resolver reference winding used in our application circuit has a resistance of 27 ohm, which leads to a 120mA peak current. The amplifier TCA0372 was chosen as driving stage, because it is capable of driving up to a 1A output current. The R5,C8 creates Boucherot circuitry that suppresses output ringing when driving inductance load. In the other type of resolver being used, it may be necessary to modify the values of R5,C8 to limit possible oscillations. Output capacitor C4 decouples the output signal dc component. Both amplifiers operate on single supply so a virtual ground is created by resistor divider R6,R7. Supply voltage VCC should be at least 2V higher than the required peak-to-peak output swing.

Driving circuitry introduces a phase shift between timer output signal and resulting resolver reference waveform. This phase shift together with resolver phase shift and signal conditioning circuitry phase shift are corrected in software by advancing the phase of the reference signal (channel TD1) relative to the ADC sampling point, which is in most motor control applications synchronized to PWM. In this way, the sampling at peaks of the sin/cos signals is ensured, resulting in better achieved resolution.

The resolver sin/cos signals conditioning circuitry adjusts voltage levels from resolver sin/cos signals to the range acceptable by the on-chip ADC module. It also carries out level shifting, which places a zero level of the signals to the middle of the ADC range. U2A, U2B amplifiers act as differential unity amplifiers with output level referenced to virtual ground (middle of the VCCA 3.3V). U2A,B amplifiers are rail-to-rail (MC33202, MC33502) or similar ones capable of 3.3V single supply operation. The capacitors C9,C12, C14,C16 add low pass filtering to suppress unwanted high frequency noise, which is often present in systems with power electronics.

The cutoff frequency of the U2A and U2B amplifiers is set according to the resolver reference frequency and should be well above it not to affect resolver signals. U2A,B amplifiers should be placed as close as possible to the ADC inputs to avoid noise crosstalk from other components.

56F80x Resolver Driver and Hardware Interface, Rev. 1
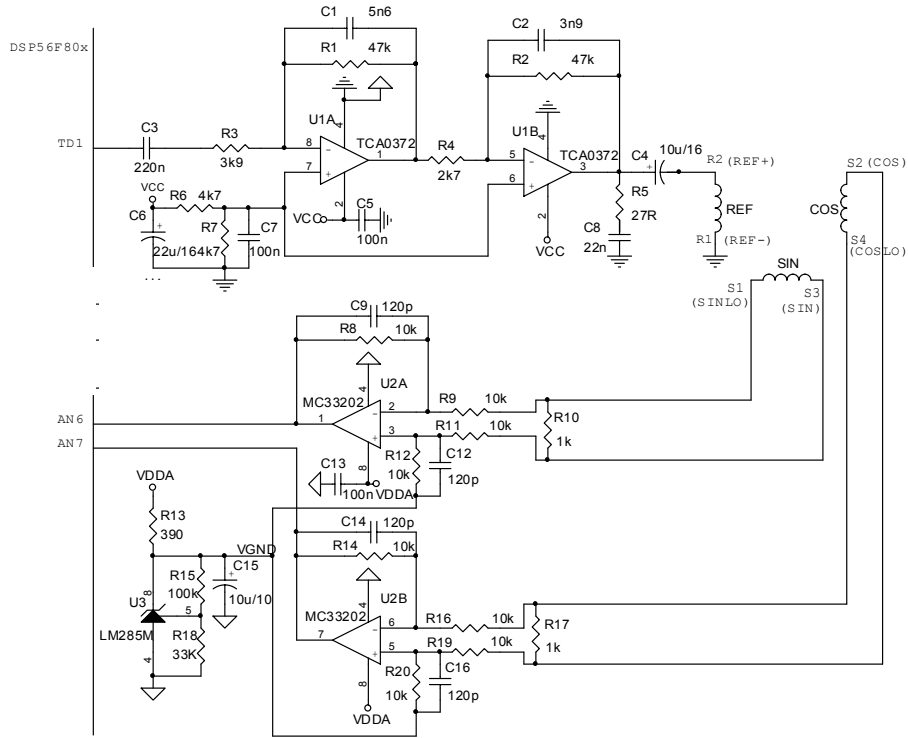
Figure 4-1. Resolver Interface Board Schematic

All values of the schematic component given in **Figure 4-1** are designed for 8kHz resolver reference frequency (half of the usual motor control PWM frequency), resolver ratio 2:1. This interface might be adjusted in cases when reference signal frequency or the resolver transformation ratio is different. The gain of the resolver signal conditioning circuitry is unity and therefore the levels on the sin/cos signal inputs must have peak-to-peak amplitude up to the ADC reference voltage (with small headroom to avoid limiting).

In case the reference frequency is different than the values of C1,R3 and C2,R4 should be adjusted to get a proper sine waveform with the needed resolver driving level. Note the ratios R1/R3 and R2/R4 have little effect on the driving level, they mainly affect the noise sensitivity of the circuit. The other possibility for changing the driving level is to use a resistor divider connected between the TD1 output and the amplifier input. The schematic explained here is suitable for direct connection to 56F805EVM boards.

5. Experimental Tests

Three sets of tests were carried out using ideal, emulated noise and real resolver signals on the 56F805 evaluation module (56F805EVM).

- Firstly, the resolver was tested to demonstrate that the *Angle Tracking Observer*, running on the 56F805EVM, is competent enough to produce fast estimations of rotor angle and rotor speed; refer to **Section 5.1**.

- Secondly, the smoothing feature of the *Angle Tracking Observer* was demonstrated; refer to **Section 5.2**.

- The third set of tests was a study of the dynamic behavior and smoothing of the *Angle Tracking Observer* in the whole application; i.e., the observer was driven by real output signals of the resolver; refer to **Section 5.3**.

5.1 Dynamic parameters of the Angle Tracking Observer

It is clear that dynamic parameters of the observer could never be obtained using the signals of the real resolver because of certain mechanical and electrical inertia of such devices. For that reason, the real resolver signals were replaced here with their ideal equivalents calculated on the device prior to observer calculation. In fact, the main goal of these tests was to find the ideal dynamic responses of the observer algorithm on step changes of the rotor angle and speed.

The dynamic responses of the *Angle Tracking Observer* were materialized using special software running on the 56F805EVM. This software was completely written in C language using the CodeWarrior 56800 development tool. The software performs the following tasks:

- It generates step changes of the resolver angle and calculates corresponding sine and co-sine resolver signals.

- It calculates the *Angle Tracking Observer* and sends calculated data (waveforms) to personal computer for printing and further post-processing.

The transient responses of the angle estimations on the step changes of the actual rotor angle are shown in **Figure 5-1**. In this case, the coefficients of the *Angle Tracking Observer* were based on the parameters of the second order system $\omega_n = 500\mathrm{rad\,s}^{-1}$, $\zeta = 0.84$, refer to **Section 3.3.3** for more details about selection of optimal observer coefficients.
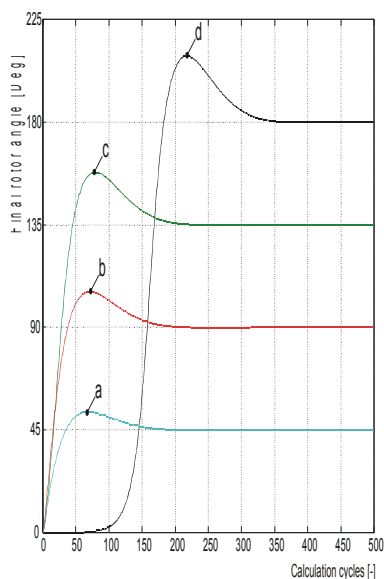
Figure 5-1. Responses of the Estimated Angle of the Angle Tracking Observer -

$$\omega_n \; = \; 500\,\text{rad s}^{-1}, \zeta = 0.84 \;.$$

The estimated rotor angle (y-axis) are illustrated versus calculation cycles (x-axis) of the *Angle Tracking Observer* algorithm.

As is known from theory of control systems, a well-designed observer tries to minimize its estimation error at every calculation cycle. In other words, observers require a certain number of calculation cycles to produce a flawless estimation. This flawless estimation means that the observer outputs reach and remain within a specified tolerance of its steady state value. This tolerance is given by the designer and considerably depends on the requirements of the particular application. Of course, the larger the tolerance the less computational cycles are required to reach a steady state.

An allowable tolerance of ±20′ (electrical) was considered. The considered tolerance corresponds to an estimation error of ±1 LSB in the case that the rotor angle is measured with 10-bit accuracy. The measured *Settling Times* and *Peak Overshoots* in terms of magnitude of the step change of the rotor angle are summarized in **Table 5-1**.

Table 5-1.   Numerical Representation of Responses - Figure 5-1.

Response Waveform	Step Change	Peak Overshoot	Settling in Calculation Cycles	Settling Time [s]
d	180°	17%	352	0.022
c	135°	17%	208	0.013
b	90°	17%	192	0.012
a	45°	17%	176	0.011

56F80x Resolver Driver and Hardware Interface, Rev. 1

The *Settling Times* are calculated considering the timing between two subsequent calculation cycles $62.5\mu s$. **Figure 5-2** shows transient responses of the rotor angle estimations on the step changes of the actual rotor angle. In this case, the coefficients of the *Angle Tracking Observer* were based on the parameters of the general second order system $\omega_n = 1200\,\text{rad s}^{-1}$, $\zeta = 0.84$.
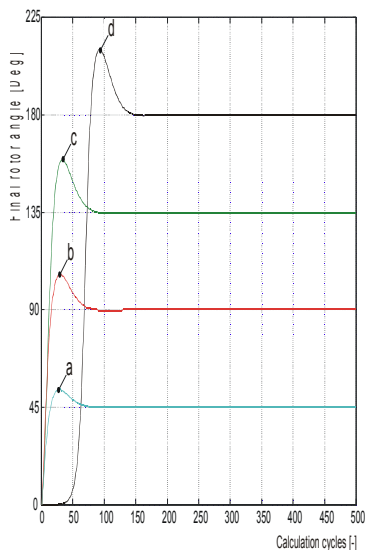
Figure 5-2.   Responses of the Estimated Angle of the Angle Tracking Observer -
$$\omega_n = 1200\,\text{rad s}^{-1}, \zeta = 0.84$$

The estimation of rotor angle (y-axis) is illustrated versus the calculation cycles (x-axis) of the *Angle Tracking Observer* algorithm. The *Settling Times* and *Peak Overshoots* in terms of magnitudes of the step changes of the rotor angle are summarized in **Table 5-2**.

Table 5-2.   Numerical Representation of Responses - Figure 5-2.

Response waveform	Step Change	Peak Overshoot	Settling in calculation cycles	Settling Time [s]
d	180°	17%	130	0.0081
c	135°	17%	90	0.0056
b	90°	17%	80	0.0050
a	45°	17%	68	0.0043

The question may arise, why the *Settling Time*s t_S, expressed here for the step changes of the rotor angle 180°, differ from those captured in **Figure 3-9** and **Figure 3-10**, despite the fact that identical parameters of the *Angle Tracking Observer* algorithm were used. This is because a different expression for calculating the estimation errors was considered. In the previous sections, the expression $\Theta - \hat{\Theta}$ was used for calculating the

estimation error - see responses for $\zeta = 0.84$ in **Figure 3-9** and **Figure 3-10**. In this case, however, the expression $\sin(\Theta - \hat{\Theta})$, reflecting the natural implementation of the *Angle Tracking Observer* algorithm, is considered (see **EQ 3-4**).

The *Settling Times* (y-axis) as a function of steady state angles (x-axis) are summarized in **Figure 5-3**. An allowable tolerance of $\pm 20'$ (electrical) was considered, which means that if the transient response of the observer lay within the tolerance, then the pending experiment was automatically stopped and the number of performed calculation cycles was recorded. This graph describes the behavior of the *Angle Tracking Observer* algorithm likewise in a real controller application - observer estimation error is calculated using the expression $\sin(\Theta - \hat{\Theta})$.
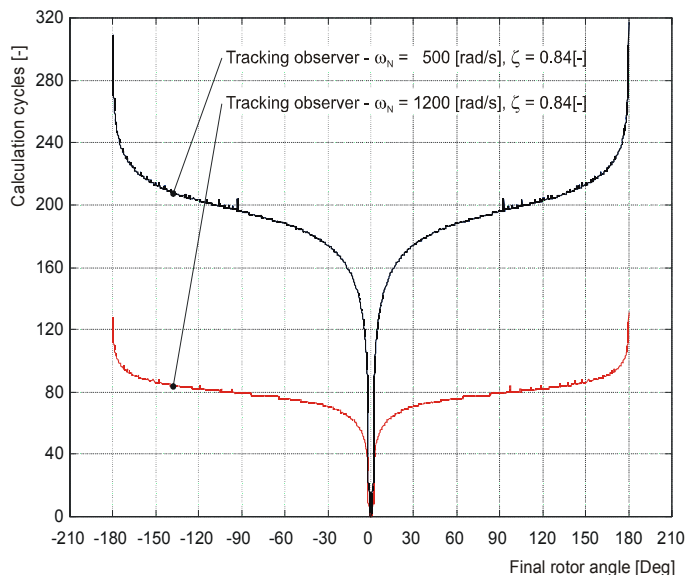
Figure 5-3.   Settling Time of the Angle Tracking Observer

The experiments discussed so far have been focused on the study of the dynamic parameters of the *Angle Tracking Observer*. The objective has been to show some effects of the parameters of the general second-order system ω_n and ζ on the dynamic behavior of the angle and speed estimations.

It has been testified that the *Settling Time* t_S varies with changes of the *Natural Frequency* ω_n and the *Damping Factor* ζ, whereas the *Peak Overshoot* OV varies solely with changes in the *Damping Factor* ζ.

5.2   Smoothing Feature of the Angle Tracking Observer

This section discusses an additional important feature of the *Angle Tracking Observer*, which is known as smoothing (filtering). It is shown that smoothing remarkably depends on the proper selection of coefficients of the *Angle Tracking Observer*.

The theory of control systems defines the hypothesis; the faster the response of the estimated variables is, the less effective their smoothing is and vice versa. This hypothesis is clearly demonstrated in **Figure 5-4**.
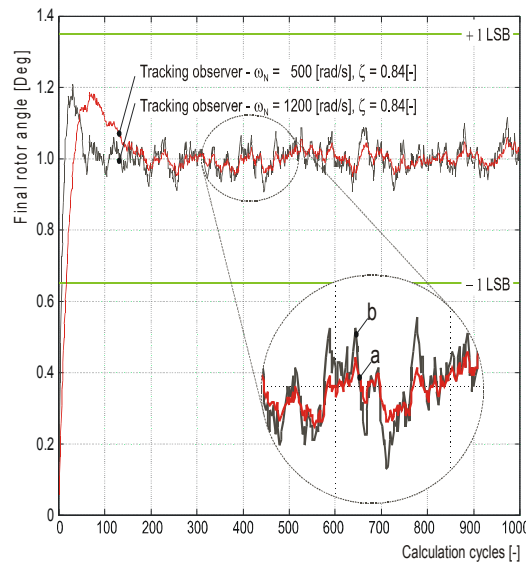
Figure 5-4. Effect of 8-bit ADC accuracy on the Accuracy of the Rotor Angle Estimation

The figure shows responses of the estimated rotor angle for 1° unit-step change of the actual rotor angle. Note that the transient responses denoted in the graph as **a** and **b**, are based on the parameters $\omega_n = 500 \text{rad s}^{-1}$, $\zeta = 0.84$ and $\omega_n = 1200 \text{rad s}^{-1}$, $\zeta = 0.84$, respectively.

Generation of the resolver output signals was performed by special software. The software also adds error into generated signals. This software feature enabled us to simulate the observer algorithm in a mode similar to its normal operation; i.e., a mode with noisy resolver output signals measured using ADC with finite accuracy. First, we tried to show the smoothing feature using simulated sin/cos signals that correspond to the ADC accuracy of the 56F80x; however, obtained waveforms did not evidently demonstrate smoothing capability due to the higher accuracy of the simulated sin/cos signals. Consequently, we decided to present more convincing waveforms. Note that introduced error is in the rank of 8-bits signal accuracy.

Figure 5-4 clearly shows that the *Angle Tracking Observer* is capable of accurate estimations even if inaccurate measurement (8-bit ADC) of the resolver output signals is carried out. Note that in both cases, the resulting final estimation error is smaller than $\pm20'$.

We have aimed so far to study the behavior of the *Angle Tracking Observer* in terms of rotor angle estimation. Advice was given for the selection of observer parameters, and discussed the dynamic and smoothing features of the angle estimation.

However, many electric drives require a precise measurement of the instantaneous rotor speed to be made. Generally, this information is obtained by differentiation of the estimated rotor angle or may be given by the *Angle Tracking Observer*. The following is the description of the dynamic behavior and smoothing features of the *Angle Tracking Observer* in terms of speed estimation.

The transient responses of estimated speed and estimation error, generated by the *Angle Tracking Observer* on the step changes of the rotor speed, are graphically illustrated in **Figure 5-5**...**Figure 5-8**.
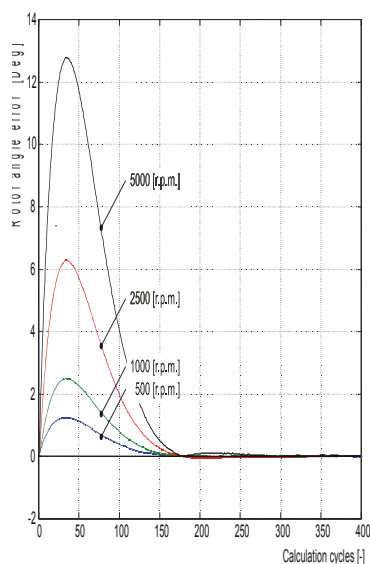
Figure 5-5 shows the transient responses of the estimated speed ñ of the *Angle Tracking Observer*, whose coefficients have been calculated on the base of parameters $\omega_n = 500 \text{rad s}^{-1}$, $\zeta = 0.84$.
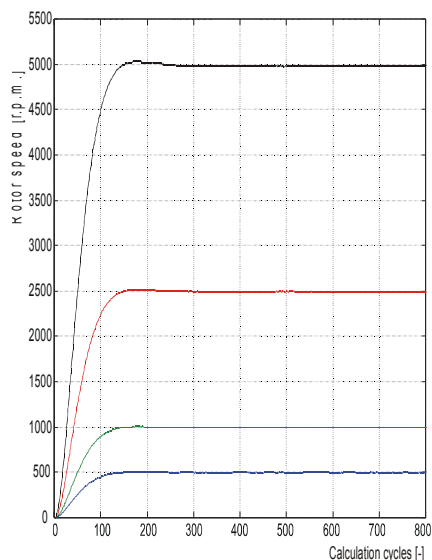
Figure 5-5.   Transient Response of Rotor Speed Estimations -
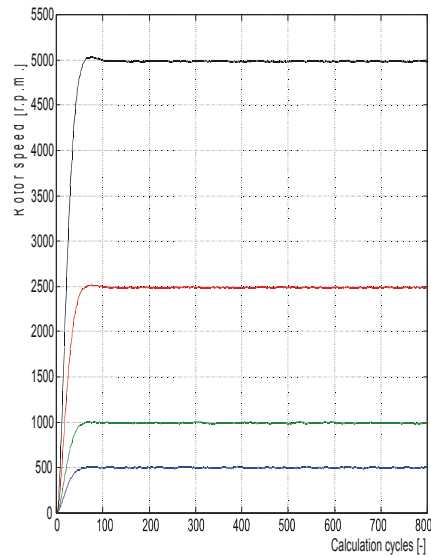$$\omega_n = 500 \text{rad s}^{-1}, \zeta = 0.84$$

Note that the estimated speed (y-axis) is expressed as a function of the calculation cycles (x-axis) of the *Angle Tracking Observer* algorithm. The depicted transient responses have settled in 160 calculation cycles, which gives - considering the time between two cycles, $62.5\mu s$ - a *Settling Time,* $t_S = 0.01s$. The *Peak Overshoot* of the transient responses is $OV < 1\%$.

Figure 5-6 expresses errors of the angle estimation $\Theta - \hat{\Theta}$ (y-axis) as a function of step changes of the rotor speed. The x-axis is in calculation cycles. The simulated Observer is based on parameters $\omega_n = 500 \text{rad s}^{-1}, \zeta = 0.84$.

Figure 5-6.   Transient Response of Rotor Angle Estimation Error -
$$\omega_n = 500 \text{rad s}^{-1}, \zeta = 0.84$$

56F80x Resolver Driver and Hardware Interface, Rev. 1

Figure 5-7 shows transient responses of the estimated speed $\hat{n}$ that have been generated by the Observer based on parameters $\omega_n = 1200\,\text{rad s}^{-1}, \zeta = 0.84$. These transient responses reach the steady state in 65 calculation cycles, which results in a *Settling Time,* $t_S = 0.0041\text{s}$. The *Peak Overshoot* of the responses is $OV < 1\%$.


Figure 5-7.   Transient Response of Rotor Speed Estimations -
$\omega_n = 1200\,\text{rad s}^{-1}, \zeta = 0.84$

Figure 5-8 expresses errors of the angle estimation $\Theta - \hat{\Theta}$ during step changes of rotor speed. Here, the *Angle Tracking Observer* is based on parameters of the general second-order system $\omega_n = 1200\,\text{rad s}^{-1}, \zeta = 0.84$.
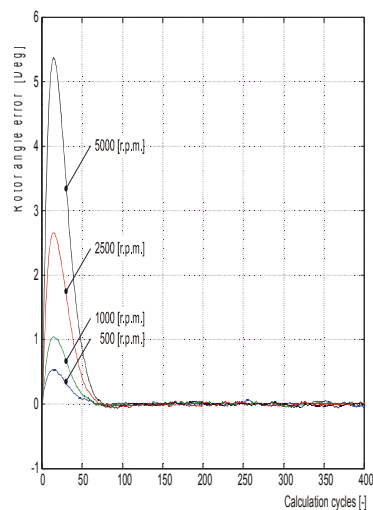
Figure 5-8.   Transient Response of Rotor Angle Estimation Error - $\omega_n = 1200\,\text{rad s}^{-1}, \zeta = 0.84$

The effect of signal noise and limited accuracy of the signal measurement on the final accuracy of the speed estimation is shown in **Figure 5-9**.
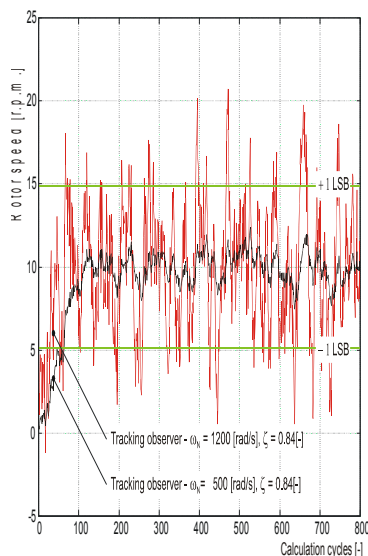
Figure 5-9. Effect of the 8-bit ADC Accuracy on the Accuracy of Rotor Speed Estimation

This figure demonstrates the smoothing capability of the Observer algorithm. Note that Observer based on parameters of the general second-order system $\omega_n = 500 \text{rad s}^{-1}$, $\zeta = 0.84$ lead to speed estimations within allowable tolerance $\pm 1 \text{LSB}$ $(\pm 0.1\%)$. Note that this tolerance is equal to the speed measurement with 10-bit resolution performed in the speed range $0 < n < 5000$ r.p.m.

While in contrast, the Observer based on parameters $\omega_n = 1200 \text{rad s}^{-1}$, $\zeta = 0.84$ provides speed estimations exceeding these limits.

The following section focuses on the demonstration of the dynamic behavior and accuracy of the *Angle Tracking Observer* driven by real resolver output signals. It will demonstrate the 56F805EVM capability of driving motor with concurrent estimation of rotor angle and speed.

5.3 Test of the Resolver Driver in a Motor Control Application

The resolver driver and hardware interface were tested in a real *Permanent Magnet Synchronous Motor*[1] (PMSM) vector control application. The hollow shaft resolver[2] and incremental encoder[3] were both mounted on the PMSM shaft, which gave us the unique capability to perform measurements of the rotor angle and speed using two independent sensors.

---

1. TGDrives, Type SBL3-0065-30-310/T0PS2X, nominal torque 0.65 Nm, nominal speed 300 r.p.m., nominal voltage 190 V, nominal current 1.05 A.
2. ATAS, Type ER5Kd 286, a two pole resolver with an electrical error ±10′, transformation ratio 0.5 ± 10%, supply voltage 7 V, max. current 50mA.
3. INDUcoder, Type ES 38-6-1024-05-D-S/I, resolution 4096 edges per shaft turn, 5 VDC, RS 422 line driver outputs.

The various tasks which are generally needed to run motor control application were executed in this application. The application handled the following tasks:

1. Calculation of the motor control algorithm, which provided for the generation of a stator voltage vector independently and in quadrature to the vector of the rotor magnetic flux.

2. Generating the switching pulses for the 3-Phase power stage. The software exploits a powerful PWM module of the controller. This module is used here to produce three complementary, individually programable, PWM signal outputs. Complementary operation permits programmable dead-time insertion, distortion correction through current sensing by software and separate top and bottom output polarity control.

3. Measurement and evaluation of encoder signals using the internal Quadrature Decoder and Quad Timer module. These modules provides for accurate measurement of the angular position, speed and number of revolutions. The measurement of angular speed and number of revolutions is carried out in 16-bit resolution.

4. The excitement of the resolver rotor winding is achieved through the Timer output. The timer automatically generates a square-wave signal that is synchronized with the motor PWM pulses. This signal is then fed through an external filter, which filters out higher harmonics and produces a sine waveform suitable for resolver excitation.

5. Measurement of the resolver output signals and estimation of the rotor angle and speed. The measurements were carried out using the ADC module that was synchronized with the generation of the PWM pulses. After completing the measurements, the device calculates new estimations of the rotor angle and speed on the base of measured resolver signals.

6. PC master software application[1] communication support.

Two types of experimental tests were carried out:

- First, the noise of the rotor angle estimation was measured and post-processed in order to reveal some dependencies.
- Second, dependence of the rotor angle estimations on the instantaneous rotor position (resolver's sine and co-sine output waveforms) was analyzed.

Figure 5-10 shows how the noise magnitude of the rotor angle estimations depends on the coefficients of the *Angle Tracking Observer*. Note that lower values of the *Natural Frequency* suppress noise and increase the smoothing capability of the observer. This figure clearly demonstrates that the *Angle Tracking Observer* approach provides for smoother estimations than the *Trigonometric* approach (red curve).

---

1. PC master software application is the debugging tool delivered together with Freescale's SDK.
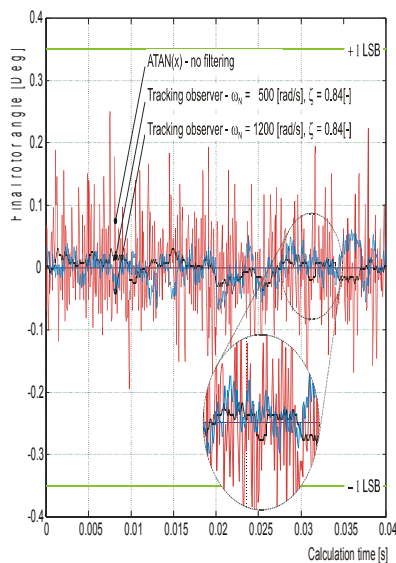
**Figure 5-10. Noise of the Rotor Angle Estimation -
Effect of Angle Tracking Observer Coefficients**

Figure 5-11 depicts the dependence of the estimation error of the rotor angle, denoted in degrees, on the instantaneous rotor position (resolver's sine and co-sine output waveforms). These curves were captured for two sets of the observer coefficients at motor speed 2500 r.p.m. It is evident that estimation errors are practically independent of the coefficients of the *Angle Tracking Observer*.
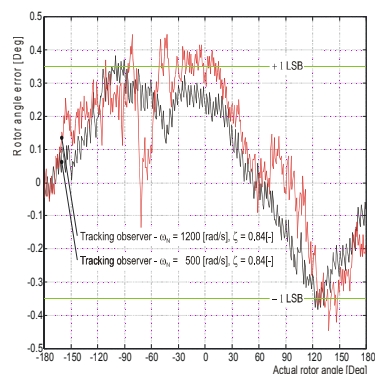
**Figure 5-11. Error and Noise of the Rotor Angle Estimation -
Effect of the Actual Rotor Angle**

56F80x Resolver Driver and Hardware Interface, Rev. 1

Note that estimation errors vary somewhat with the rotor angle. These imperfections are mainly formed from two sources.

- The first source are undoubtedly imperfections in the two-pole resolver. The accuracy of the exploited resolver, guaranteed by the manufacturer, is ± 0.15 electrical degree.
- The second source of errors is imperfections in the calibration of the external conditioning hardware (see **Section 4.**) and ADC integral nonlinearity.

The smoothing feature of the *Angle Tracking Observer* in terms of speed estimation is shown in **Figure 5-12**. The figure shows waveforms of speed estimation, carried out at standstill mode for two sets of the observer coefficients. Note that the *Angle Tracking Observer*, whose coefficients were designed using $\omega_n = 500 \text{rad s}^{-1}$, $\zeta = 0.84$, performed an adequate smoothing of the estimated speed.

On the contrary, the *Angle Tracking Observer* based on parameters $\omega_n = 1200 \text{rad s}^{-1}$, $\zeta = 0.84$ performed inadequate smoothing; some values lie outside the allowable range. The term adequate smoothing means here that all estimations of the rotor speed lay within the allowable range ± 1 LSB $(\pm 0.1\%)$.

As shown in the magnified part of the **Figure 5-12**, the observer can estimate satisfactory speed waveforms in terms of accuracy. Nevertheless, it is also apparent that estimated waveforms contain higher harmonics, which would never occur in reality due to the certain mechanical time constants of the real rotor. These harmonic components arise because of the substantial sensitivity of the Observer speed estimation loop to the inaccuracies in the signal measurement. This sensitivity, however, must naturally be high in order to ensure fast convergence of the position estimation process. Note that too high sensitivity of the speed loop (pole is too far in the left half plane) results in a large observer coefficient which may cause saturation problems, instability and observer bandwidth increases. The bandwidth increases can cause a noise problem. Hence, proper judgement has to be used by the designer [5].
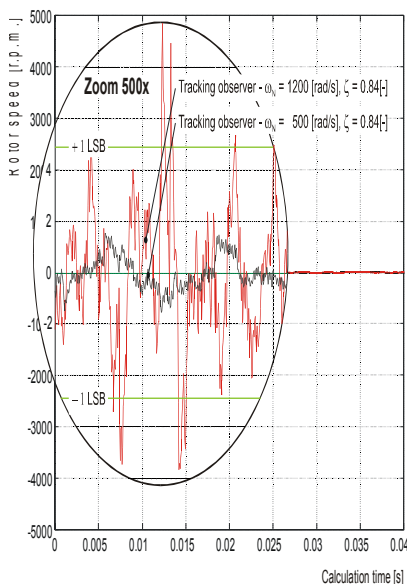
**Figure 5-12. Noise of the Rotor Speed Estimation -
Effect of Angle Tracking Observer Coefficients**

56F80x Resolver Driver and Hardware Interface, Rev. 1

Note that ordinarily an additional filtering of the rotor speed estimates is mostly incorporated in the real application whenever achieving smoother waveforms is crucial without compromise on the dynamic of the position estimation.

The accuracy and smoothing of estimated variables may further be refined utilizing automatic calibration of inaccuracies in the external hardware interface, a more accurate resolver sensor and tailoring observer coefficients. The approach of selecting optimal observer coefficients is given in **Section 3.3.3**. Even more, **Figure 3-11** and **Figure 3-12** graphically illustrate variations of the *Peak Overshoot* and *Settling Time* in terms of the *Natural Frequency* and *Damping Factor* of the observer.

6. Conclusion

Hollow Shaft Resolvers are position sensors with high resistance to distortion, mechanical shocks and vibrations, deviations in operating temperature and dust in a wide range with practically unlimited durability. Among further advantages are low price, simple assembly and easy maintenance. In the case of two pole resolvers the absolute position is given immediately after starting up. Thanks to resolvers' advantages and their mass production, they are presently used in numerous electric drive applications. Their popularity is demonstrated by the remarkable growth of their worldwide application, starting from thousands of pieces in 1990 to millions pieces at the present.

It was demonstrated that Freescale's 56F805, together with the resolver hardware and software interface, allows users to fully utilize resolver features and also permits cost reductions of final applications by achieving a single chip solution. The system design is simplified utilizing the versatile functionality of the Quad Timer and ADC on-chip modules together with a powerful core.

The Freescale 40 MIPS 56F80x family provides enough computational power to perform Resolver-to-Digital conversion in parallel to sophisticated digital control algorithms, like the demonstrated PMSM vector control application. The computational load by the resolver driver is approximately 7.5%; the rest is fully available for the user application.

Besides the presented features, the 56F80x family offers functions that satisfy a variety of motor control applications in terms of computational power, PWM generation, ADC, timers, communication modules, etc. The reliability and safety is maintained at a high degree by features like PWM fault protection and detection of Low-Voltage, Loss of PLL Lock and Loss of PLL Clock.

7. References

[1.] Petr Kohl, Tomas Holomek, Hollow Shaft Resolvers - Modern Position Sensors, ATAS Elektromotory a.s. Nachod, project report, 2000

[2.] Don Morgan - Tracking Demodulation - Embedded Systems Programming, n. 1, January 2001, pp. 115-120.

[3.] Norman S. Nise. - Control System Engineering, The Benjamin Icummings Publishing Company, California State Polytechnic University, 1995

[4.] Mohammed S. Santina, Allen R. Stubberud, Gene H. Hostetter - Digital Control System Design - Chapter 5 "Digital Observer and Regulator Design", International Thomson Publishing, 1994

[5.] Bahram Shahian, Nichael Hassul - Control System Design Using Matlab - Chapter 8.3 "Observer Design", Prentice Hall, Englewood Cliffs, 1993

How to Reach Us:

Home Page:
www.freescale.com

E-mail:
support@freescale.com

USA/Europe or Locations Not Listed:
Freescale Semiconductor
Technical Information Center, CH370
1300 N. Alma School Road
Chandler, Arizona 85224
+1-800-521-6274 or +1-480-768-2130
support@freescale.com

Europe, Middle East, and Africa:
Freescale Halbleiter Deutschland GmbH
Technical Information Center
Schatzbogen 7
81829 Muenchen, Germany
+44 1296 380 456 (English)
+46 8 52200080 (English)
+49 89 92103 559 (German)
+33 1 69 35 48 48 (French)
support@freescale.com

Japan:
Freescale Semiconductor Japan Ltd.
Headquarters
ARCO Tower 15F
1-8-1, Shimo-Meguro, Meguro-ku,
Tokyo 153-0064, Japan
0120 191014 or +81 3 5437 9125
support.japan@freescale.com

Asia/Pacific:
Freescale Semiconductor Hong Kong Ltd.
Technical Information Center
2 Dai King Street
Tai Po Industrial Estate
Tai Po, N.T., Hong Kong
+800 2666 8080
support.asia@freescale.com

For Literature Requests Only:
Freescale Semiconductor Literature Distribution Center
P.O. Box 5405
Denver, Colorado 80217
1-800-441-2447 or 303-675-2140
Fax: 303-675-2150
LDCForFreescaleSemiconductor@hibbertgroup.com

AN1942
Rev. 1
08/2005